

**Sn(IV) Schiff Base Complexes: Triplet Photosensitizers for Photoredox Reactions**

Journal:	<i>Dalton Transactions</i>
Manuscript ID:	DT-ART-05-2014-001427.R1
Article Type:	Paper
Date Submitted by the Author:	03-Jul-2014
Complete List of Authors:	Grusenmeyer, Tod; Tulane University, Chemistry King, Albert; Ohio University, Chemistry and Biochemistry Mague, Joel; Tulane University, Chemistry Rack, Jeffrey; Ohio University, Department of Chemistry Schmehl, Russel; Tulane University, Department of Chemistry

Sn(IV) Schiff Base Complexes: Triplet Photosensitizers for Photoredox Reactions

*Tod A. Grusenmeyer^A; Albert W. King^B; Joel T. Mague^A; Jeffrey J. Rack^B; Russell H. Schmehl^{*A}*

^ADepartment of Chemistry, Tulane University, New Orleans, Louisiana 70118, United States

^BDepartment of Chemistry and Biochemistry, Ohio University, Athens, Ohio 45701, United States

We present the synthesis and characterization of a series of four fluorescent Sn(IV) Schiff base complexes, which also possess long-lived triplet excited states. The complexes absorb visible light ($\lambda_{\text{max}} = 420$ to 462 nm) and the optical properties are easily tunable without laborious synthetic elaboration. The triplet excited states are not luminescent, but can be observed and followed using nanosecond transient absorption spectroscopy. The lifetimes of the triplet excited states are on the order of $500 \mu\text{s} - 10$ ms in PMMA matrices. The triplet state energies were estimated via energy transfer reactions with a series of organic triplet acceptors. In addition, the photoexcited complexes react with electron donors and acceptors in solution. These results demonstrate the potential for the development of photosensitizers based on main group elements with high spin orbit coupling constants.

Keywords. Tin Schiff Base Complexes, Luminescence, Transient Absorbance, Triplet State Photochemistry, Photoinduced Energy Transfer, Photoinduced Electron Transfer

Introduction

There has been a great deal of work on exploiting transition metal complex chromophores as sensitizers in artificial photosynthetic systems for conversion and storage of solar energy. The majority of such systems rely on the sensitizer to serve as a single electron donor or acceptor following visible light excitation. These chromophores are typically second and third row transition metal complexes because they have excited state lifetimes in the microsecond time regime, often exhibit stability in multiple oxidation states, and are luminescent, allowing both the excited state energy and lifetime to be determined conveniently. The desirable, relatively long excited state lifetimes result from the fact that the photoactive excited states are all of triplet spin multiplicity while the ground states are of singlet multiplicity. The formation of triplet excited states is facilitated by the presence of the metal due to large spin-orbit coupling matrix elements that enhance intersystem crossing. The majority of published work focuses on complexes of Ru(II), Os(II), Ir(III), Re(I) and Pt(II). A common criticism of artificial photosynthetic systems involving these complexes has been the relative scarcity of these elements; all are among the nine rarest elements in the earth's crust.

A clear challenge for the photochemistry community is the development of complexes that have redox and photophysical properties similar to those used in existing artificial photosynthetic systems, but employ earth-abundant metals. Our intent is to utilize complexes that are easily prepared and have visible electronic transitions. The objective for the metal is to use an element with a large spin-orbit coupling matrix element (similar to the noble metals) that forms complexes that are stable in multiple oxidation states. Also, as a pedagogical point of interest, we wanted to investigate molecules that may contain non-phosphorescent long-lived excited states. In this regard, it appeared that complexes of either Sn(II) or Sn(IV) might be appropriate since

Sn is relatively abundant in the earth's crust and has a spin-orbit coupling matrix element significantly greater than that of Ru, which is widely used in metal complex sensitizers¹.

There are a number of articles addressing the photoreactivity of Sn complexes in the literature. These reports mainly focus on the photochemistry of Sn(II) and Sn(IV) aquo, halide, hydroxo, and cluster complexes²⁻⁸, Sn porphyrins⁹⁻²⁸, phthalocyanines²⁹⁻³³, and corroles³⁴⁻³⁷, and transition metal complexes utilizing organotin compounds as a ligand³⁸⁻⁴⁷. The simple Sn(IV) complexes (halides, hydroxo, etc.) typically absorb in the ultraviolet, do not luminesce and exhibit irreversible photochemistry from LMCT excited states. Sn(II) complexes mainly access metal based s→p type excited states, some of which are luminescent at room temperature. Octahedral Sn(II) clusters also access s→p metal based excited states. These clusters show a red shift in their luminescence due to metal-metal bonding interactions. Sn(II)/Sn(IV) halide bridged dimers have also been investigated and are known to exhibit MMCT transitions. Metal-to-Ligand Charge Transfer (MLCT) transitions are observed in Sn(II) bpy complexes and porphyrins. The literature on Sn porphyrins, phthalocyanines and corroles is extensive and includes reports of catalytic hydrogen reduction, sensitization in organic solar cells, and donor-acceptor arrays. Sn macrocycles are also known to efficiently sensitize singlet oxygen and have been used in schemes for pollutant remediation and photodynamic therapy; here the excited states are largely localized on the macrocycle. Given these Sn complexes as a basis and recognizing both the rich redox chemistry and the extraordinarily large spin-orbit coupling coefficient of Sn, recent reports of a series of fluorescent Sn(IV) Schiff base derivatives with visible absorption^{48, 49} appeared to be an excellent entrée for investigation of triplet state formation and reactivity in Sn(IV) complexes.

Results

Four tin complexes containing tridentate Schiff-Base ligands, $[\text{PhSn}(\text{Lnap})\text{Cl}_2]$, $[\text{PhSn}(\text{Lsal})\text{Cl}_2]$, $[\text{PhSn}(\text{LBr})\text{Cl}_2]$, and $[\text{PhSn}(\text{Ldea})\text{Cl}_2]$; HLnap is 2-hydroxy-1-naphthaldehyde-8-aminoquinoline, Hlsal is salicylaldehyde-8-aminoquinoline, HLBr is 5-bromosalicylaldehyde-8-aminoquinoline, and HLdea is 4-diethylaminosalicylaldehyde-8-aminoquinoline) were synthesized and investigated. The ligands are prepared via an imine forming condensation reaction of 8-aminoquinoline with various salicylaldehyde derivatives and 2-hydroxy-1-naphthaldehyde. The complexes were prepared in a one pot process via the addition of Ph_2SnCl_2 to a solution of the freshly prepared ligand in toluene. As the reaction progresses, the tin complex precipitates from solution. HLnap was independently prepared for characterization by reaction of the 2-hydroxy-1-naphthaldehyde with 8-aminoquinoline in absolute ethanol as previously reported.⁵⁰ The crystal structure of one complex, $[\text{PhSn}(\text{Lnap})\text{Cl}_2]$, and the other ligands reacted with Ph_2SnCl_2 are shown in Figure 1. Crystal structures have also been obtained for the other complexes and ORTEP representations of each molecule are presented in Supporting Information (Figures S21-S24), each confirming the trans geometry of the chloride ligands. The complexes were further characterized by ^1H NMR spectroscopy; the spectra clearly indicate ^{119}Sn (8.59%) and ^{117}Sn (7.68%) coupling to the ortho protons of the tin bound phenyl ring and the imine proton of the various NNO ligands. Other coupling assignments were made using ^1H - ^1H COSY. Images of ^1H NMR spectra are included in Supporting Information (Figures S1-S5).

X-ray Crystallography. Selected bond lengths and angles are presented in Table 1. The two Sn coordinated nitrogen atoms are distinguished as the quinoline nitrogen, N_Q , and the imine nitrogen (linking the quinoline and the aldehyde), N_I . In addition, the Sn-N and Sn-Cl bond

lengths for tetraphenylporphinatodichlorotin(IV) ([SnTPPCl₂]) as well as the bond lengths and angles obtained from the DFT geometry optimized singlet ground state are presented in Table 1. In crystals of [PhSn(LBr)Cl₂], there are three independent conformers in the asymmetric unit and they differ primarily in the dihedral angle between the mean planes of the phenyl group and the SnN₁Cl₂ unit (15.5°, 34.2° and 37.4°). The bond lengths and angles for these conformers are given in Table 1 as [PhSn(LBr)Cl₂] (1), [PhSn(LBr)Cl₂] (2), and [PhSn(LBr)Cl₂] (3), respectively. The Sn-N₁ and the Sn-N_Q bond lengths are similar for all of the molecules in the series. The shortest Sn-N₁ bond length of 2.167(1) Å and longest Sn-N_Q bond length of 2.242(2) Å both occur in [PhSn(Ldea)Cl₂]. All of the other Sn-N bond lengths fall within this 0.06 Å window and are approximately 0.1 Å longer than the Sn-N bonds in [SnTPPCl₂]. All of the Sn-C bonds are slightly shorter than the Sn-N bonds. The Sn-C bonds in [PhSn(Lnap)Cl₂], [PhSn(Lsal)Cl₂], and [PhSn(Ldea)Cl₂] are all similar with lengths of 2.146(2) Å, 2.151(2) Å, and 2.146(2) Å, respectively. For the set of [PhSn(LBr)Cl₂] conformers, the Sn-C bond lengths are equivalent within experimental error, ranging from 2.137(3) Å to 2.145(3) Å. The Sn-O bond lengths are the shortest of all of the bonds in the coordination environment and are in the very narrow range 2.036(2) Å - 2.050(2) Å. The Sn-Cl bond lengths are significantly longer with values ranging from 2.4430(7) Å to 2.4996(4) Å. These are slightly longer than the Sn-Cl bond lengths observed in [SnTPPCl₂]. All of the crystallographically determined bond lengths are in good agreement with those obtained from DFT calculations. The most notable difference is in the determination of the Sn-Cl bond lengths where gas phase DFT calculations yield bond lengths that are roughly 2.5% longer than in the crystallized molecules.

The Cl-Sn-Cl bond angle is significantly less than 180° with the Cl atoms displaced away from the phenyl ring towards the imine nitrogen of the ligand such that the SnN₁Cl₂ unit is nearly

planar. The departure of the Cl-Sn-Cl angle from 180° is dependent on the dihedral angle between the phenyl ring and the mean SnN_1Cl_2 plane. In $[\text{PhSn}(\text{Lsal})\text{Cl}_2]$, this angle is 13.3° , resulting in a Cl-Sn-Cl bond angle of $166.85(2)^\circ$. In contrast, when this angle increases to 21.3° in $[\text{PhSn}(\text{Ldea})\text{Cl}_2]$ and 28.0° in $[\text{PhSn}(\text{Lnap})\text{Cl}_2]$ the Cl-Sn-Cl bond angle increases to $169.24(2)^\circ$ and $169.74(2)^\circ$, respectively. For the series of $[\text{PhSn}(\text{LBr})\text{Cl}_2]$ conformers observed in the asymmetric unit, as the dihedral angle increases from 15.5° to 37.4° the Cl-Sn-Cl bond angle increases from $166.78(3)^\circ$ to $168.36(3)^\circ$. The distortions from this geometry seen in the solid state structures can be seen to be due in part to contacts between the *o*-hydrogens on the phenyl group and the axial chlorine atoms. With the smallest dihedral angles these contacts are in the range $2.60 - 2.76 \text{ \AA}$ which is about that of a normal van der Waals contact (2.74 \AA).⁵¹ The larger Cl-Sn-Cl and dihedral angles involve $\text{H}\cdots\text{Cl}$ contacts in the range $2.8 - 3.0 \text{ \AA}$. Although an exhaustive analysis of the packing has not been performed, it appears that the observed Cl-Sn-Cl and dihedral angles represent the best balance between minimizing the intramolecular $\text{H}\cdots\text{Cl}$ contacts and intermolecular contacts involving the phenyl ring which affect the dihedral angle. The O-Sn-N_Q bond angles vary from $159.15(7)^\circ$ in $[\text{PhSn}(\text{Lnap})\text{Cl}_2]$ to $163.55(5)^\circ$ in $[\text{PhSn}(\text{Ldea})\text{Cl}_2]$. As the dihedral angle between the plane of the phenyl ring and the SnN_1Cl_2 plane increases in $[\text{PhSn}(\text{LBr})\text{Cl}_2]$, the O-Sn-N_Q bond angle increases from $159.56(8)^\circ$ to $161.43(9)^\circ$. There also is a slight disparity in the C-Sn-N_I bond angles across the series of molecules. $[\text{PhSn}(\text{Lnap})\text{Cl}_2]$ and $[\text{PhSn}(\text{Lsal})\text{Cl}_2]$ have similar C-Sn-N_I bond angles of $170.60(8)^\circ$ and $170.05(8)^\circ$. $[\text{PhSn}(\text{LBr})\text{Cl}_2]$ and $[\text{PhSn}(\text{Ldea})\text{Cl}_2]$ have slightly larger C-Sn-N_I bond angles of $172.9(1)^\circ$ and $172.14(6)^\circ$. Variations in the phenyl plane/ SnN_1Cl_2 dihedral angle do not affect the C-Sn-N_I bond angle in the series of $[\text{PhSn}(\text{LBr})\text{Cl}_2]$ conformers. The DFT calculated values for O-Sn-N_Q bond angles are all in very good agreement with the values

obtained from the crystal structures. The calculated values for C-Sn-N_I are also in good agreement with the crystal structure values other than for [PhSn(Lnap)Cl₂] where the calculated bond angle is 3° larger than the observed value. The calculated values for the Cl-Sn-Cl bond angles are not in good agreement with observed values. All of the calculated values are at least 3° less than the actual bond angles.

Steady-State Absorption and Luminescence. The complexes are all yellow or orange in solution. The electronic absorption spectra of the complexes in acetonitrile are shown in Figure 2 with maxima and extinction coefficients given in Table 2. The HLnap ligand has two overlapping absorption bands (450nm and 473nm) while the complex has a single maximum at 452nm. The HLnap ligand and all of the Sn(IV) complexes exhibit luminescence in acetonitrile. The fluorescence of [PhSn(Lnap)Cl₂] is ~100 times greater than the HLnap ligand (Figure S10). It is also important to note that [PhSn(Ldea)Cl₂] is the only complex in the series that shows fluorescence solvatochromism (Figure S11), exhibiting a red shift with increasing solvent polarity and suggesting that the singlet excited state of this complex has significant charge transfer character. Fluorescence quantum yields of the complexes in acetonitrile range from 0.14 for [PhSn(Lnap)Cl₂] to 0.01 for [PhSn(Ldea)Cl₂] suggesting the possibility of significant intersystem crossing to the triplet manifold. There is no evidence of phosphorescence in fluid solution or 77K glass. The fluorescence lifetimes for the complexes were also determined by TCSPC. The instrument response function (scatter), raw luminescence decay, and the exponential fit of the deconvoluted luminescence decay of [PhSn(Lsal)Cl₂] are shown in Figure S34. Collected lifetimes are given in Table 2 for all of the complexes except [PhSn(Ldea)Cl₂] which has a decay that is faster than the resolution of our system (~ 300 ps). The fluorescence

lifetimes and quantum yields for our series of chromophores are similar to values previously reported for closely related $[\text{SnLCl}_3]$ complexes.^{48, 49}

Nanosecond Transient Absorption. Each chromophore has a unique, long-lived excited state absorption in de-aerated acetonitrile, which was assumed to be associated with the triplet state of the chromophore. The transient absorption spectrum of $[\text{PhSn}(\text{Lnap})\text{Cl}_2]$ at room temperature along with the ground state absorption over the same spectral window is shown in Figure 3. The key features of these spectra are bleaching of the ground state absorption and excited state absorption at all wavelengths to the red of 500 nm. The spectrum has three isobestic points and individual decays indicate a small (<5%) degree of permanent product formation. The dashed spectrum of Figure 3 indicates the changes observed in the ground state absorption following collection of the transient spectrum further indicating photodegradation in acetonitrile. Transient absorption spectra for the other complexes are shown in Figures S13-S15. Solution transient decays were non-exponential, regardless of complex concentration, and were best fit using equal concentration second order kinetics, suggesting that triplet-triplet annihilation dominates excited state relaxation in solution. Given the observed solution behavior involving collisional reaction processes, the excited state decay dynamics were examined in solid poly(methyl methacrylate) matrices (PMMA). In PMMA, the transient absorption decays are single exponential and have lifetime values of 570 μs for $[\text{PhSn}(\text{LBr})\text{Cl}_2]$, 1.1 ms for $[\text{PhSn}(\text{Lsal})\text{Cl}_2]$, 980 μs for $[\text{PhSn}(\text{Lnap})\text{Cl}_2]$, and 11.9 ms for $[\text{PhSn}(\text{Ldea})\text{Cl}_2]$.

Detailed analysis of the solution kinetics required knowledge of excited state molar concentrations. The excited state absorptivities and yields for triplet state formation were obtained from experiments involving triplet energy transfer to an acceptor with a known excited state absorptivity (anthracene) using solutions that were absorbance matched with $[\text{Ru}(\text{bpy})_3]^{2+}$

at the excitation wavelength (allowing determination of the total concentration of excited states from the absorbance of the $[\text{Ru}(\text{bpy})_3]^{2+}$ triplet absorbance; see experimental). The decay data was converted from absorbance units using the triplet-triplet extinction coefficients for each chromophore. The excited state decays were then fit using equal concentration second order kinetics. The intrinsic decay rate constants of the triplet Sn complex, k_r and k_{nr} , are orders of magnitude smaller than $k[\text{Sn}^*]^2$, even at the lowest complex concentrations able to be used in the transient absorbance experiments. The equal concentration second order kinetic rate constants are similar for all chromophores and range from 1.60×10^{10} for $[\text{PhSn}(\text{Ldea})\text{Cl}_2]$ to 2.01×10^{10} for $[\text{PhSn}(\text{Lsal})\text{Cl}_2]$.

Ultrafast Transient Absorption. The femtosecond transient absorption spectrum of $[\text{PhSn}(\text{Lnap})\text{Cl}_2]$ in N_2 de-aerated acetonitrile at room temperature is shown in Figure 4. Spectra of the remaining complexes are shown in Figures S16-18. A summary of the kinetic information for the spectra is compiled in Table 2. In aggregate, all four complexes feature tri-exponential kinetics, with the longest lived transient spectrum (~ 3200 ps) resembling the earliest transient spectrum from the nanosecond studies, illustrating continuity between the time regimes examined. For all four complexes, there is a fast sub-picosecond kinetic component ranging from about 100 fs to 800 fs. We ascribe this to an internal conversion process of the initially formed excited state. The long time kinetic phase for the complexes ranges from 15 ps (most rapid) to 2500 ps (most slow). Transient spectra over this time regime have isosbestic points and exhibit the loss of narrow peaks or structure to yield broad features. This kinetic component corresponds to relaxation of the singlet excited state to yield either ground state or triplet. The lifetimes of this component (Table 3) match well with the singlet lifetimes obtained by TCSPC (Table 2). In addition, all four complexes have a kinetic component that is intermediate in time (between sub-

picosecond and the long time kinetic components), ranging from 1 to 70 ps for the different complexes. This kinetic phase is difficult to assign, but, for all the complexes, a rise in optical density and a blue shift of excited state absorption feature(s) is observed after the sub-picosecond kinetic process.

Triplet Yields and Energies. Triplet state energies of the complexes were obtained by energy transfer quenching with a series of triplet acceptors in acetonitrile. The collected energy transfer rate constants were used in evaluation of the free energy dependence of the rate constants using the classical treatment of energy transfer in fluid solution.⁵²⁻⁵⁴ Free energy dependence plots are shown in Figures S19 and 20 with the resulting triplet state energies given in Table 2. While the results only allow an estimate of the triplet energy to be obtained, a clear trend in behavior is easily noted. The [PhSn(Lsal)Cl₂] and [PhSn(LBr)Cl₂] have triplet energies of 16500cm⁻¹ and 16300cm⁻¹, respectively. The triplet state energies of these complexes are approximately 500cm⁻¹ higher than [PhSn(Ldea)Cl₂] and [PhSn(Lnap)Cl₂].

As mentioned above, intersystem crossing yields for population of triplet excited states were obtained by sensitization of a triplet with a known excited state absorptivity (anthracene) and comparison with a known standard [Ru(bpy)₃]²⁺ (see Experimental). This experiment results in a range of efficiencies: 0.72 for [PhSn(LBr)Cl₂], 0.59 for [PhSn(Lsal)Cl₂], 0.36 for [PhSn(Lnap)Cl₂], and 0.05 for [PhSn(Ldea)Cl₂].

Singlet Oxygen Sensitization. The triplet states of these complexes are also capable of sensitizing the formation of ¹O₂. The collection of excited state lifetime measurements in the presence of oxygen allowed for the determination of a bimolecular quenching rate constants in CH₃CN, which were 2 x 10⁹ M⁻¹s⁻¹ for all complexes. Further, the quantum yield of singlet oxygen formation was determined from the near infrared ¹O₂ phosphorescence in air saturated

solutions of each of the chromophores and comparing them to an absorbance matched air saturated $[\text{Ru}(\text{bpy})_3]^{2+}$ standard solution ($\Phi = 0.57^{55}$). The quantum yields for singlet oxygen sensitization are 0.43 for $[\text{PhSn}(\text{Lnap})\text{Cl}_2]$, 0.52 for $[\text{PhSn}(\text{Lsal})\text{Cl}_2]$, and 0.66 for $[\text{PhSn}(\text{LBr})\text{Cl}_2]$. These values parallel the observed triplet yield efficiencies. No $^1\text{O}_2$ phosphorescence was observed from $[\text{PhSn}(\text{Ldea})\text{Cl}_2]$ sensitization; this is likely due to the extremely low triplet yield for the complex.

Photoinduced Electron Transfer Reactions: A key question relating to this class of complexes is the ability of the chromophores to serve as either excited state electron donors or acceptors. An estimate of the excited state oxidizing and reducing ability can be obtained from the energy of the triplet excited state and the electrochemical potentials obtained from cyclic voltammetry. Cyclic voltammograms of the complexes indicate that neither oxidation nor reduction is reversible at sweep rates up to the limit of our instrumentation (2 V/s; Figures S6-S9). Approximate potentials based upon anodic and cathodic peak maxima were determined and are given in Table 1. The reduction potentials for all of the complexes are similar and have approximate values of -1.3 V vs. Ag/AgCl. The oxidation potentials for $[\text{PhSn}(\text{LBr})\text{Cl}_2]$, $[\text{PhSn}(\text{Lsal})\text{Cl}_2]$, and $[\text{PhSn}(\text{Lnap})\text{Cl}_2]$ are all similar and occur around 1.3V. As expected, $[\text{PhSn}(\text{Ldea})\text{Cl}_2]$ is much easier to oxidize with a potential of 0.83 V. Given that the triplet excited state energy for all chromophores is approximately 2 eV ($16,100 \text{ cm}^{-1}$), a crude estimate of the $[\text{PhSn}(\text{L})\text{Cl}_2]^{*/-}$ potential is +0.70 for all chromophores. For excited state oxidation, the $[\text{PhSn}(\text{L})\text{Cl}_2]^{+/*}$ potential is -0.70 V for $[\text{PhSn}(\text{LBr})\text{Cl}_2]$, $[\text{PhSn}(\text{Lsal})\text{Cl}_2]$, and $[\text{PhSn}(\text{Lnap})\text{Cl}_2]$ and -1.2 V for $[\text{PhSn}(\text{Ldea})\text{Cl}_2]$ vs Ag/AgCl, suggesting the complexes can serve as modest one-electron acceptors and donors. To provide a test of photoredox reactivity, reductive quenching with 10-methyl-phenothiazine (MPTH, $E^0(+/0) = 0.7 \text{ V}$ vs. Ag/AgCl) and oxidative quenching

with methyl viologen (MV, $E^0(2+/+) = -0.44\text{V}$ vs. Ag/AgCl) was carried out in CH_3CN solutions.

Transient spectra obtained in acetonitrile in the presence of MPTH and MV are shown in supplementary information (Figures S31-S32) for all the complexes. For reductive quenching measurements with MPTH, the absorbance signal between 510 and 550 nm is clearly indicative of the MPTH cation radical and is observed for all the complexes. Rate constants for quenching with MPTH are $9 \times 10^9 \text{ M}^{-1}\text{s}^{-1}$ for $[\text{PhSn}(\text{LBr})\text{Cl}_2]$, $7 \times 10^9 \text{ M}^{-1}\text{s}^{-1}$ for $[\text{PhSn}(\text{Lsal})\text{Cl}_2]$, $6 \times 10^9 \text{ M}^{-1}\text{s}^{-1}$ for $[\text{PhSn}(\text{Lnap})\text{Cl}_2]$, and $1 \times 10^9 \text{ M}^{-1}\text{s}^{-1}$ for $[\text{PhSn}(\text{Ldea})\text{Cl}_2]$. Quenching with methyl viologen also yielded transient spectra that strongly resemble the $\text{MV}^{+\bullet}$ ion with strong absorption at 395 nm and a broad absorption band with a maximum centered at 600 nm. Quenching rate constants with methyl viologen are $7 \times 10^8 \text{ M}^{-1}\text{s}^{-1}$ for $[\text{PhSn}(\text{LBr})\text{Cl}_2]$, $1 \times 10^9 \text{ M}^{-1}\text{s}^{-1}$ for $[\text{PhSn}(\text{Lsal})\text{Cl}_2]$, $2 \times 10^9 \text{ M}^{-1}\text{s}^{-1}$ for $[\text{PhSn}(\text{Lnap})\text{Cl}_2]$, and $\sim 1 \times 10^{10} \text{ M}^{-1}\text{s}^{-1}$ for $[\text{PhSn}(\text{Ldea})\text{Cl}_2]$. Control experiments of excitation in the absence of chromophore resulted in no transient absorbance in the visible. Back electron transfer rate constants for all chromophores are diffusion limited with both MV and MPTH.

Given the observation of long-lived triplet state formation and photoredox reactivity for the Sn(IV) complexes, possible energy and electron transfer photoreactivity for the free ligands alone was examined. The transient absorption spectrum of the HLnap ligand in de-aerated acetonitrile as well as transient absorption spectra of the ligand in the presence of 9mM 9-bromoanthracene and 1mM MPTH are shown in Figure S12. A transient species clearly remains in the ligand spectrum after 3 milliseconds; however, this species is not quenched by either MPTH or 9-bromoanthracene.

Discussion

Ligand Behavior. Given the similarity of the absorption and fluorescence data of the ligands and the Sn(IV) complexes, the possibility exists that the observed behavior for the complexes is essentially a simple extension of the behavior of the free ligand. A search of the literature does not yield any previous microsecond to millisecond transient absorption results for any of the ligands or complexes, although steady state and ultrafast experimental work has been done on HLnap. As a starting point it is useful to discuss the structurally related molecule salicylideneaniline (SalAn, made from the condensation of salicylaldehyde and aniline). An interesting feature of this and HLnap that differs from the Sn(IV) complexes is contribution of a keto tautomeric form which can exist in E and Z stereoisomeric forms with respect to the C-N imine linkage as shown in Figure 5. The ground state absorption spectrum of SalAn does not absorb above 400nm and is invariant with changes in solvent polarity. The UV absorption bands in the SalAn spectrum are attributed to absorbance of the ground state enol tautomer. By contrast, there is a clear solvent dependence of the ground state absorption spectrum of another Schiff base, naphthylideneaniline (NapAn, made from the condensation of 2-hydroxynaphthaldehyde and aniline); two absorption bands appear above 400nm as the solvent polarity increases. This change in absorbance is ascribed to the formation of keto tautomer in solution. It is clear that both the keto and enol form of NapAn are present in polar solvents.⁵⁶ The ground state absorption spectrum of the HLnap ligand features two strong absorption bands above 400nm and the absorption spectrum is unchanged in solvents of varying polarity; this is attributed to a stabilization of the keto form through hydrogen bonding with the quinoline nitrogen (Figure 5).⁵⁷ The photochromic nature of the SalAn excited state was initially described in the 1960's in the crystalline state⁵⁸, low temperature matrices⁵⁹, and solution^{59, 60}. These initial

reports assign this photochromic state as a ground state E NH structure (Figure 5). Subsequent literature reports have examined the kinetic evolution of the excited state of salicylideneaniline⁶¹⁻⁶⁷ in fluid solution. Excitation of the enol form of SalAn results in sub-picosecond intramolecular proton transfer to form the fluorescent, keto, form followed by relaxation to a ground state species with either a cis-zwitterionic (iminium ion/ naphthoate) or the isomerized E NH structure. This latter isomeric species has a lifetime of 400 μ s in acetonitrile.

The absorption, luminescence and femtosecond time-resolved absorption spectrum of the HLnap ligand has also been reported.^{68, 69} The ultrafast spectroscopic behavior consists of three spectral features of note: (1) two well defined bleaching bands corresponding to both of the local maxima in the ground state absorption spectrum at 450nm and 475nm that decay via a multi-exponential path that includes a very long lived component (> 5 ns), (2) an intense, broad absorption between 500-620nm, containing two peaks at 525nm and 580nm that disappear over 30 ps, and (3) stimulated emission at wavelengths to the red of 620nm that decays with a rate constant of 4 ps. The authors conclude that the behavior can be explained by processes that involve excitation of the Z NH (Figure 5) ground state followed by decay of the initially formed vibronic state (relatively high in the manifold) to a mix of the S_1 and S_2 states of the Z NH conformer over 700 fs. Stimulated emission of the S_1 state occurs over the first 4 ps, during which time a long lived state is formed; meanwhile the S_2 state decays to the ground state with a lifetime of 13ps. The long lived state (> 5 ns) is attributed by the authors to formation of either a Z NH triplet or possibly the E NH isomer. The key postulate relating to the two components of the ultrafast behavior is the formation and relatively slow (13 ps) decay out of the S_2 state directly back to the ground state without relaxation to the S_1 state. In addition, formation of the E NH isomer postulated for the HLnap is highly unlikely in the Sn(IV) complexes.

Excited States and Kinetics of the Sn(IV) Complexes. As mentioned above, the absorption and luminescence spectra of HLnep and the $[\text{PhSn}(\text{Lnep})\text{Cl}_2]$ are similar, suggesting a strong correspondence of the orbitals and states involved. The HOMO and LUMO obtained from DFT geometry optimized structures of the Sn(IV) complexes, shown in Figures S25-S28, clearly illustrate that neither the Sn(IV) nor the coordinated phenyl contribute in any significant way to the HOMO or LUMO of any of the complexes. Small contributions to the HOMO from the coordinated Cl are seen for all the complexes other than $[\text{PhSn}(\text{Ldea})\text{Cl}_2]$.

The ultrafast transient spectral data for the complexes other than $[\text{PhSn}(\text{Ldea})\text{Cl}_2]$ have common spectral features that differ from those of the nanosecond transients but evolve over a few nanoseconds to a final spectrum that closely corresponds to the longer time transients (> 10 ns). Thus, the sub-nanosecond kinetics results in the formation of the long lived triplet. Two of the three dynamic components of the decays of the ultrafast transients can be classified: the subpicosecond decay is likely due to vibrational relaxation of the singlet manifold and the longest decay corresponds to relaxation of the singlet excited state (to triplet and ground state). The intermediate component varies from 70 ps for $[\text{PhSn}(\text{Lnep})\text{Cl}_2]$ to 1 ps for $[\text{PhSn}(\text{Ldea})\text{Cl}_2]$, with the other two complexes closer to $[\text{PhSn}(\text{Lnep})\text{Cl}_2]$. The time for all but the Ldea complex is much too long for solvation of the excited state and the explanation for such a long process is not clear. It is possible that the initial excitation may lead to population of two different singlet states that decay with vastly different rate constants. In support of this is the observation that the ultrafast spectrum does not really change during the 40 - 100 ps time period over which the intermediate component decays.

The luminescence lifetime values for the complexes obtained from TCSPC measurements are in good agreement with the long component of the decay of the ultrafast transient absorption

spectrum for all chromophores. These values reflect the decay of the initially formed singlet excited state by radiative, non-radiative, and intersystem crossing processes. Using the experimentally obtained lifetime value, quantum yield of intersystem crossing, and the quantum yield of fluorescence, the rate constants of all three relaxation processes can be determined.

The rates of intersystem crossing vary from $2.6 \times 10^8 \text{ s}^{-1}$ for $[\text{PhSn}(\text{Lnap})\text{Cl}_2]$ to $9.0 \times 10^8 \text{ s}^{-1}$ for $[\text{PhSn}(\text{LBr})\text{Cl}_2]$. The intersystem crossing rate of $[\text{PhSn}(\text{LBr})\text{Cl}_2]$ is 3 times greater than that of $[\text{PhSn}(\text{Lnap})\text{Cl}_2]$ and $[\text{PhSn}(\text{Ldea})\text{Cl}_2]$, and only slightly greater than that of $[\text{PhSn}(\text{Lsal})\text{Cl}_2]$. This implies that presence of a second heavy atom (Br) does not have a large effect on the observed rate of intersystem crossing. It is also important to note that the intersystem crossing rates for chromophores of this type are four orders of magnitude slower than those of well-known ruthenium polypyridyl chromophores. The radiative decay rates of the singlet state only differ by a factor of two across the series of four chromophores from $1.0 \times 10^8 \text{ s}^{-1}$ for $[\text{PhSn}(\text{Lnap})\text{Cl}_2]$ to $5.0 \times 10^7 \text{ s}^{-1}$ for $[\text{PhSn}(\text{Lsal})\text{Cl}_2]$ and are in the range of radiative decay rate constants of organic chromophores with allowed $\pi\text{-}\pi^*$ transitions.

The largest difference in rate constants of the singlet excited states is observed for the non-radiative decay rate of $[\text{PhSn}(\text{Ldea})\text{Cl}_2]$, which is an order of magnitude faster than the non-radiative decay rates for all of the other molecules in the series. It is perhaps not surprising that the ultrafast absorption spectrum is fundamentally different from the other three complexes, lacking completely the absorption feature that appears immediately upon excitation between 350 and 400 nm and remains. The solvent dependence of the absorption and luminescence behavior indicates that the excited singlet state has significant charge transfer character and relaxation of this excited state is the fastest of the four complexes ($k_{\text{nr}} = 6 \times 10^9 \text{ s}^{-1}$). The effect of this is

reflected in a relatively low quantum yield for fluorescence *and* a very low intersystem crossing efficiency.

Since none of the complexes exhibit phosphorescence from the long-lived transient absorbing species, a systematic effort was made to assign the transients. Examination of quenching of the long lived transients with a series of triplet quenchers (Figures S19-20) indicated a systematic dependence of the quenching rate constant on the triplet energy of the quencher. The data were fit assuming a reversible energy transfer model⁵²⁻⁵⁴ and the triplet energies (Table 2) obtained indicate a relatively small range for the complexes. Interestingly, the energy gaps between the singlet states (taken from the fluorescence maxima) and the triplet states are 3800 cm^{-1} , 2500 cm^{-1} , 2300 cm^{-1} and 1100 cm^{-1} for the Lnap, Lsal, LBr and the Ldea complexes, respectively. For the first three the relative efficiencies for populating the triplet state increase with decreasing S_1-T_1 gap, but the 4deaesal complex has a very low η_{isc} despite an apparently small S_1-T_1 gap. However, the observed fluorescence originates from a state with a large degree of charge transfer character and the triplet may well represent a state that is more similar to the other complexes in electron distribution. At this point, we have no data that relates to the degree of charge transfer character in the triplet state of the Ldea complex, but the low intersystem crossing efficiency observed, despite the small apparent S_1-T_1 gap, clearly indicates a fundamental difference between this complex and the others.

The triplet energies of all the complexes are well above that of singlet oxygen and near-infrared emission spectra of aerated solutions of all the complexes other than the Ldea complex clearly showed the signature 1270 nm emission of singlet oxygen. Yields for oxygen formation were between 40 and 60% in acetonitrile. The lack of sensitized singlet oxygen emission in the Ldea complex is attributed to the very low yield of triplet states in this complex.

Electron transfer quenching experiments with an electron donor and electron acceptor with clearly identifiable radical ion absorbance in the visible ($\text{MPTH}^{+\bullet}$ and $\text{MV}^{+\bullet}$) served to illustrate the potential of the complexes to serve as both excited state oxidants and reductants. For reductive quenching with MPTH, the transient absorption spectrum following electron transfer quenching should reflect the sum of the radical ion species absorption less the absorption of the ground state complex and quencher (MPTH). Since MPTH has no visible absorbance and the absorption spectra of the starting complex and the MPTH cation radical are known, the only remaining unknown is the spectrum of the one-electron reduced form of the Sn complex. The voltammetric data clearly indicate that reduction of the complex is irreversible (probably E_1C_1 process), thus we were unable to obtain the spectrum of the reduced complex by spectroelectrochemistry. However, it should be noted that the transient spectra obtained following quenching with MPTH (Figure S31) *strongly* resemble spectra generated from the difference of the MPTH cation radical and the Sn complex ground state absorption. The implication is that the absorbance of the reduced Sn complex in the visible is minimal, possibly suggesting reduction of the metal (to Sn(III)) rather than ligand localized reduction to make the ligand anion radical, which would very likely have strong visible absorption. However, the DFT results (Figures S25-S28) clearly suggest that the LUMO is ligand localized. The back reaction of the reduced complex with the $\text{MPTH}^{+\bullet}$ is observed, but over the course of the acquisition of a transient absorption spectrum the $\text{MPTH}^{+\bullet}$ begins to accumulate in solution, indicating decomposition of the reduced Sn complex occurs on the hundreds of microseconds time scale.

A similar behavioral trend was observed upon quenching with an oxidative quencher, MV: the transient spectrum of the long lived species resembled the difference between the MV cation

radical absorbance and the ground state absorption of the complex. All the complexes served as effective one-electron donors, with the Ldea complex being the most effective. While we have no direct evidence, it is likely the oxidized complex reflects the ligand cation radical (see the HOMO of DFT in Figures S25-S28). As above, back electron transfer occurs, but some decomposition of the oxidized Sn complex occurs on the time scale of the back reaction and reduced viologen gradually accumulates in solution.

Summary. The synthesis and characterization of a series of four fluorescent Sn(IV) Schiff base complexes with reasonably high yields of triplet state formation is described. The complexes absorb in the visible ($\lambda_{\text{max}} = 420$ to 462 nm) and their optical properties are easily tunable without laborious synthetic elaboration. The complexes are fluorescent, with low emission yields, and also form nonluminescent triplet excited states with formation yields ranging from 5 % to 70%. Ultrafast transient spectral studies provide lifetimes for the singlet excited states, with decays that correlate well with luminescence followed by TCSPC. The triplets were observed and kinetically evaluated using nanosecond transient absorption spectroscopy. The lifetimes of the triplet excited states are on the order of 500 μs – 10 ms in PMMA matrices. Triplet-triplet annihilation processes occur at near diffusion limited rates in solutions of the chromophores. The triplet state energies were estimated from the free energy dependence of energy transfer rate constants for reaction with a series of organic triplet acceptors. All the complexes other than the Ldea complex were good sensitizers for singlet oxygen emission. The photoexcited complexes react with both electron donors and acceptors in solution, although decomposition of both the complex radical anion and radical cation competes to some degree with back electron transfer. These results demonstrate the potential for the

development of photosensitizers based on main group elements with high spin orbit coupling constants.

Experimental Details

Syntheses. Ph_2SnCl_2 , 8-aminoquinoline, 2-hydroxy-1-naphthaldehyde, salicylaldehyde, 5-bromosalicylaldehyde, and 4-diethylaminosalicylaldehyde were all purchased from Sigma-Aldrich and used as received. Acetonitrile, absolute ethanol, diethylether, hexanes and toluene were obtained from Pharmco-AAPER and used as received.

2-hydroxy-1-naphthaldehyde-8-aminoquinoline (HLnap). The ligand 2-hydroxy-1-naphthaldehyde-8-aminoquinoline was synthesized as previously reported.⁵⁰ 1g (6.9mmol) 8-aminoquinoline and 1.19g (6.9 mmol) 2-hydroxy-1-naphthaldehyde were added to 40 ml absolute ethanol and allowed to stir for 12 hours. 2-hydroxy-1-naphthaldehyde-8-aminoquinoline precipitates as the reaction progresses. The solid was isolated on fritted glass and washed with 25ml cold absolute ethanol. 1.92g (93% yield) of orange solid obtained. ^1H NMR (CDCl_3) δ ppm: 9.29 (1H, d, 11.1Hz), 9.08 (1H, d, 2.8Hz), 8.20 (d, 1H, 7.28Hz), 8.00 (1H, d, 8.28Hz), 7.77 (1H, d, 7.32Hz), 7.68 (2H, m), 7.60 (2H, m), 7.51 (2H, m), 7.28 (1H, d, 7.48Hz), 6.91 (1H, d, 9.44Hz).

PhSn(Lnap)Cl_2 . 66.3 mg (4.6×10^{-4} mol) 8-aminoquinoline and 99.4 mg (4.6×10^{-4} mol) 2-hydroxy-1-naphthaldehyde were added to 15 ml toluene and refluxed for 15 h. The reaction was removed from heat and allowed to cool to room temperature. 160 mg (4.6×10^{-4} mol) Ph_2SnCl_2 was added to the reaction vessel. The toluene was removed via rotary evaporation and the resulting orange precipitate was collected on fritted glass, washed with hexanes (30ml) and diethylether (15ml), and dried in vacuo. 229.5 mg (89% yield) of orange solid was obtained. The synthesis of the salicylaldehyde containing derivatives were carried out in identical fashion. ^1H

NMR (CD₃CN) δ ppm: 9.90 (1H, s, 48.7Hz), 8.85 (1H, d, 7.88Hz), 8.55 (1H, d, 4.16Hz), 8.49 (2.17H, m), 8.33 (1.65, d, 6.16 Hz), 8.17 (1.17H, d, 8.24), 8.08 (2H, m), 7.87 (2H, m), 7.69 (1H, t, 7.84Hz), 7.62 (3H, m), 7.48 (1H, t, 7.44Hz), 7.01 (1H, d, 9.16).

PhSn(Ldea)Cl₂. 74.3 mg (5.2×10^{-4} mol) 8-aminoquinoline, 99.4mg (5.2×10^{-4} mol) 4-diethylaminosalicylaldehyde, and 189.5 mg (5.5×10^{-4} mol) Ph₂SnCl₂ were used in the synthesis. 246.8 mg (81% yield) of red solid was obtained. ¹H NMR (CD₃CN) δ ppm: 8.74 (1H, d, 7.84Hz), 8.70 (1H, s, 50.5Hz), 8.42 (1.14H, d, 4.08Hz), 8.32 (1.65H, d, 7.48Hz, 60.1Hz), 8.14 (1.15H, d, 7.60Hz), 7.97 (2H, m), 7.74 (2H, dd, 3.4Hz, 7.08Hz), 7.57 (3H, m), 7.37 (1H, d, 9.24Hz), 6.48 (1H, d, 9.20Hz), 5.96 (1H, s), 3.47 (4H, q, 7.12), 1.19 (6H, t, 7.08).

PhSn(Lsal)Cl₂. 90 μ l salicylaldehyde (8.2×10^{-4} mol), 121.2mg (8.4×10^{-4} mol) 8-aminoquinoline, and 288.2 mg (8.4×10^{-4} mol) Ph₂SnCl₂ were used in the synthesis. 301.5mg (71%) of yellow solid was obtained. ¹H NMR (CD₃CN) δ ppm: 9.19 (1H, s, 44.0Hz), 8.82 (1H, d, 8.04Hz), 8.50 (1H, d, 4.24Hz), 8.41 (1H, d, 7.80Hz), 8.29 (0.14H, 1.70H, 0.14H, d, 7.52Hz, 59.5Hz), 8.20 (1H, d, 8.28Hz), 8.02 (1H, t, 8.12), 7.81 (1H, dd, 4.96Hz, 8.28Hz), 7.67 (1H, d, 7.12Hz), 7.60 (5H, m), 6.98 (1H, t, 7.44Hz), 6.84 (1H, d, 8.48Hz).

PhSn(LBr)Cl₂. 106.7 mg 5-bromosalicylaldehyde (5.3×10^{-4} mol), 74.2 mg (5.1×10^{-4} mol) 8-aminoquinoline, and 177.3 mg (5.2×10^{-4} mol) Ph₂SnCl₂ were used in the synthesis. 235.6mg (78%) of yellow solid was obtained. ¹H NMR (CD₃CN) δ ppm: 9.12 (1H, s, 43.6Hz), 8.83 (1H, d, 7.88Hz), 8.50 (1H, d, 4.36Hz), 8.39 (1.19H, d, 7.88Hz), 8.27 (1.68H, d, 6.12Hz, 62.0Hz), 8.23 (1H, d, 9.60Hz), 8.11 (0.12H), 8.03 (1H, t, 7.84Hz), 7.81 (2H, m), 7.60 (4H, m), 6.79 (1H, d, 8.76Hz).

Spectroscopy. ¹H and 2D-COSY NMR spectra were recorded on a Varian 400 MHz NMR.. UV-vis absorption spectra were obtained on a Hewlett-Packard 8452A diode array

spectrophotometer. Photoluminescence spectra were obtained using a PTi Quantamaster spectrophotometer fit with a Hamamatsu R928 PMT detector.

Nanosecond Time-Resolved Transient Absorption. Nanosecond transient absorption measurements were performed using a Qunatel Brilliant B Q-switched Nd:YAG laser-pumped OPO (Opotek) as the pump source at a right angle to the analyzing light source. Excitation pulses were <5ns. An Applied Photophysics LKS.60 laser flash photolysis spectrometer was used for detection; the instrument is equipped with a 150 W pulsed Xe arc lamp as the analyzing light source, a single grating monochromator (Applied Photophysics 0.25m) after the sample, and PMT detection (Hamamatsu R928). The output was recorded on an Agilent Infinium transient digitizer. Decays and spectra were acquired and analyzed with Applied Photophysics LKS.60 software.

The quantum yield of triplet state formation was determined for the series of complexes using a $[\text{Ru}(\text{bpy})_3]^{2+}$ standard and photosensitization of anthracene. The change in optical density of a sample of $[\text{Ru}(\text{bpy})_3]^{2+}$ at 370nm resulting from a 10mJ pulse of 450nm laser light was determined. Using the excited state molar absorptivity of $[\text{Ru}(\text{bpy})_3]^{2+}$ at 370nm⁷⁰, the concentration of triplet excited states can be calculated. Samples of each chromophore were absorbance matched with the $[\text{Ru}(\text{bpy})_3]^{2+}$ standard and quenched with a 0.01M solution of anthracene in acetonitrile. The resulting change in absorbance at 420nm⁷¹ allows for the determination of the concentration of anthracene triplet formed. The concentration of excited anthracene is equal to the number of Sn complex triplet excited states created in the laser pulse. The ratio of Sn triplet excited states created to the number of $[\text{Ru}(\text{bpy})_3]^{2+}$ triplet excited states created gives the quantum yield of triplet state formation.

Femtosecond Time-Resolved Transient Absorption. Femtosecond transient absorption measurements were collected on an Ultrafast Systems HELIOS transient absorption spectrometer. A Spectra Physics Solstice laser, a one-box regenerative amplifier containing a Mai Tai femtosecond oscillator and Empower pump laser, was employed to produce 800nm pulses at a repetition rate of 1kHz at 3.5 W average power and a pulse width of <100fs. From this unit, the beam is split (50:50) with one beam directed to an optical parametric amplifier (TOPAS, Light Conversion) and the other to the HELIOS spectrometer (He-vis-3200) to create the pump (TOPAS) and probe (HELIOS) sources, respectively. The 800nm probe beam passed through a CaF₂ plate to generate a white light continuum (~330-700nm). The spectrum was integrated for 2 s each scan. The pump and probe beams were directed to a 2 mm path length cuvette containing the sample where they were spatially overlapped. The solution was vigorously stirred in the 2 mm path length cuvette during data collection. Transient absorption data were corrected by subtracting spectral background features that persisted from the previous pulse and appeared prepulse as well as applying chirp correction and T0 corrections using Surface Explorer Pro 1.1.5 software (Ultrafast Systems).

Time Correlated Single Photon Counting (TCSPC). Luminescence lifetimes were obtained using the time correlated single photon counting technique. Each sample was excited using an IBH NanoLED pulsed diode laser source (441nm excitation, 200ps pulse width). The emitted light was collected at right angle to the excitation pulse and collected by an IBH Model TBX-04 cooled photomultiplier (PMT) detector. The output of the PMT served as the input for the stop channel of the time to amplitude converter (TAC, Tennelec TC-863). Start pulses for the TAC were obtained from the synchronous TTL output of the NanoLED laser source. The output from the TAC was directed to the multichannel analyzer (Ortec, Easy MCA) where the signal was

accumulated. Laser light scattered from the nonluminescent solution was used to accumulate instrument response profiles. The data were analyzed using the deconvolution routine in Origin 9.

Cyclic Voltammetry. Cyclic voltammetry was performed on a CH Instruments CH1730A Electrochemical Analyzer. The working electrode was a glassy-carbon electrode, the counter electrode was a Pt wire, and the reference electrode was a Ag/AgPF₆ in acetonitrile electrode. All cyclic voltammetry data was collected in acetonitrile solutions containing 0.1M TBAPF₆. All samples were bubble degassed with argon for 10 minutes prior to collection. The presented sweep segments presented in supporting information (Figures S6-9) were collected at a scan rate of 100 mV/s.

Computational Details. DFT calculations were performed using the Gaussian 09 software package.⁷² All calculations were performed at the B3LYP level of theory, and utilized the LANL2DZ basis set with the electron core potentials of Hay and Wadt for Sn⁷³ and the 6-31G(d,p) basis set for all other atoms. No imaginary vibration frequencies were observed, confirming the validity of the geometry optimized structures.

Supporting Information. ¹H NMR DATA, Cyclic Voltammetry, Room Temperature Luminescence, Nanosecond Transient Absorption, Ultrafast Transient Absorption, Saltiel Plots, ORTEP Representations, Illustrations of calculated HOMO and LUMO orbitals, Transient Absorption decays, ¹O₂ Phosphorescence, Time Correlated Single Photon Counting Data and the determination of Intersystem Crossing Efficiencies are available as supplementary information.

Acknowledgment. The authors wish to thank the U.S. Department of Energy, Office of Chemical Sciences (Grant DE-FG-02-96ER14617) for support of this research. JR acknowledges

support of the National Science Foundation under Grants CHE 0809699, 0947031, and 1112250.

TG wishes to thank the Louisiana Board of Regents for a Graduate Fellowship.

Figures

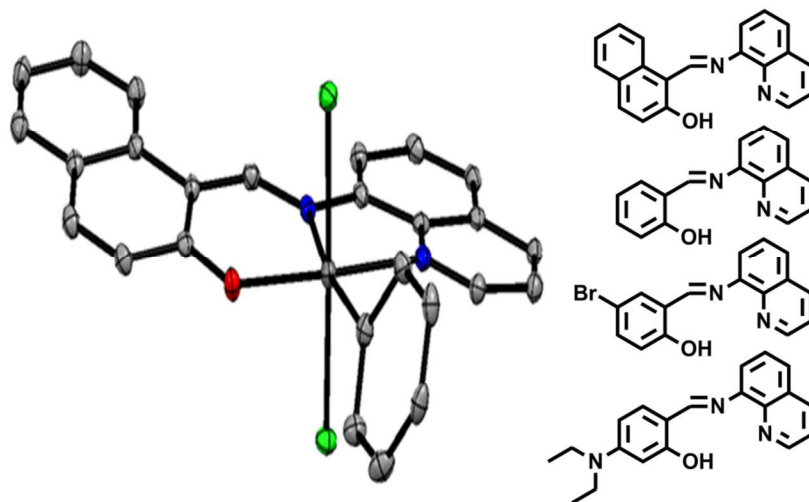


Figure 1. Left: Thermal ellipsoid plot (50% probability) of the complex PhSn(Lnap)Cl₂. Hydrogen atoms are omitted for clarity. A labeled ORTEP representation and table of crystallographic information is presented in supporting information. Right: The ligands reacted with Ph₂SnCl₂ (Top to Bottom) HLnap, Hlsal, HLBr, HLdea.

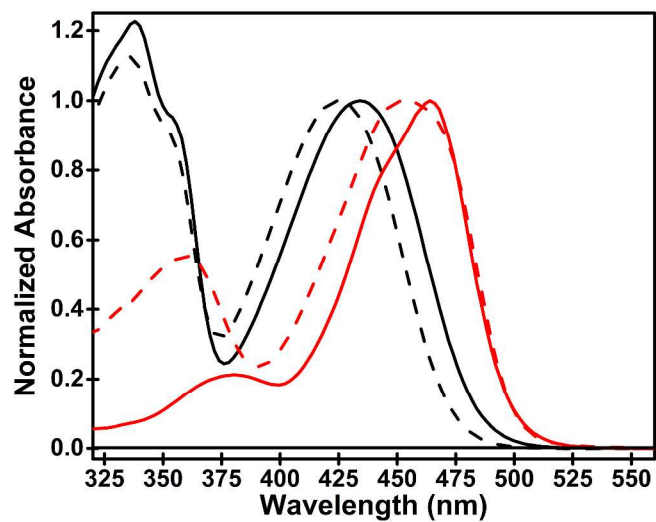


Figure 2. Absorption spectra of $[\text{PhSn}(\text{Lsal})\text{Cl}_2]$ (---), $[\text{PhSn}(\text{LBr})\text{Cl}_2]$ (—), $[\text{PhSn}(\text{Lnap})\text{Cl}_2]$ (---), and $[\text{PhSn}(\text{Ldea})\text{Cl}_2]$ (—) in acetonitrile.

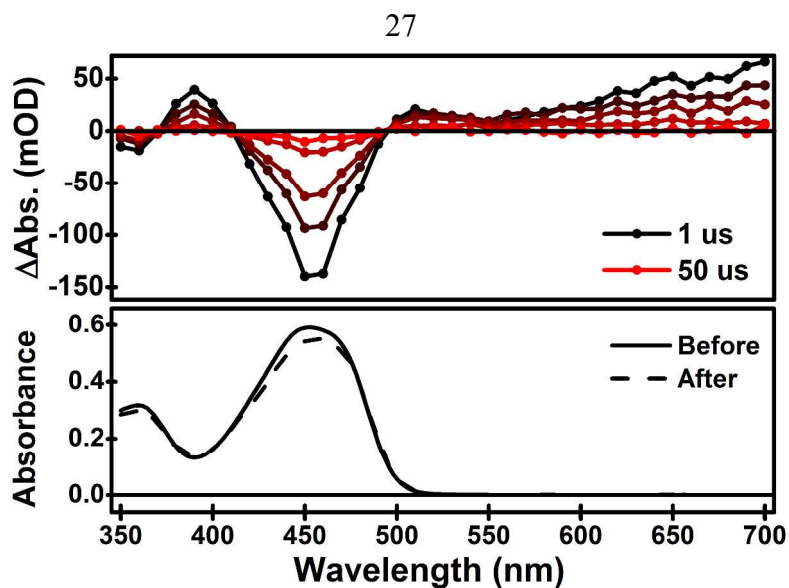


Figure 3. (Top) Transient absorption spectrum of $[\text{PhSn}(\text{Lnap})\text{Cl}_2]$ collected 1 μs , 5 μs , 10 μs , 25 μs , and 50 μs after excitation with a 450nm laser pulse. TA spectra of the remaining complexes are provided in Supporting Information. (Bottom) UV-Visible absorption spectrum collected before (—) and after (---) the collection of the TA spectrum.

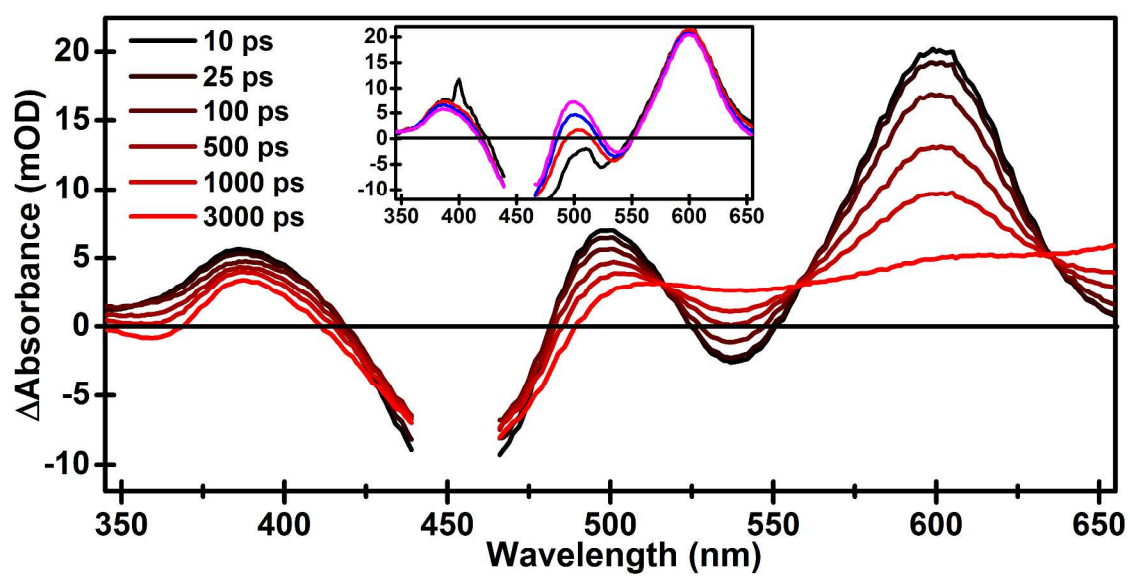


Figure 4. Ultrafast transient absorption spectrum of [PhSn(Lnap)Cl₂] in acetonitrile. Inset: Early time traces 0.300 ps (—), 0.500 ps (—), 1 ps (—), and 5 ps (—). Evidence of the laser pulse has been omitted for clarity.

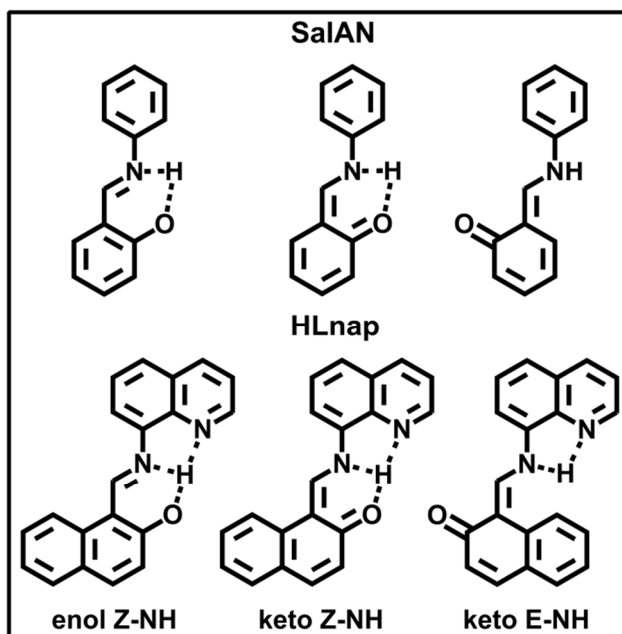


Figure 5. Structural representations of possible tautomers and stereoisomers of SalAn and HLnap.

Tables

Table 1. Selected Bond Lengths.

Complex	[PhSn(Lnap) Cl ₂]	[PhSn(Lsal) Cl ₂]	[PhSn(LBr) Cl ₂] (1)	[PhSn(LBr) Cl ₂] (2)	[PhSn(LBr) Cl ₂] (3)	[PhSn(Ldea) Cl ₂]	[SnTPPCl ₂] ⁷⁴
Sn-N _I (Imine)	2.196(2) [2.199]	2.220(2) [2.227]	2.230(2) [2.234]	2.214(2) [2.234]	2.205(2) [2.234]	2.167(1) [2.204]	2.098(2)
Sn-N _Q (Quinoline)	2.233(2) [2.244]	2.230(2) [2.248]	2.230(2) [2.244]	2.236(2) [2.244]	2.235(3) [2.244]	2.242(2) [2.251]	
Sn-C	2.146(2) [2.147]	2.151(2) [2.146]	2.145(3) [2.144]	2.137(3) [2.144]	2.140(3) [2.144]	2.146(2) [2.150]	
Sn-O	2.045(2) [2.028]	2.036(2) [2.014]	2.033(2) [2.018]	2.050(2) [2.018]	2.036(2) [2.018]	2.036(1) [2.012]	
Sn-Cl	2.4761(6) [2.5330] 2.4676(6) [2.5298]	2.4755(7) [2.5320] 2.4430(7) [2.5264]	2.4723(8) [2.5275] 2.4625(8) [2.5232]	2.4716(8) [2.5275] 2.4632(7) [2.5232]	2.4670(8) [2.5275] 2.4424(8) [2.5232]	2.4996(4) [2.5403] 2.4691(4) [2.5342]	2.420(1)
Cl-Sn-Cl Bond Angle	169.74(2) [165.71]	166.85(2) [164.11]	166.78(3) [163.97]	167.66(3) [163.97]	168.36(3) [163.97]	169.24(2) [165.14]	
O-Sn-N _Q Bond Angle	159.15(7) [159.75]	161.49(7) [161.45]	159.56(8) [161.37]	160.95(8) [161.37]	161.43(9) [161.37]	163.55(5) [162.37]	
C-Sn-N _I Bond Angle	170.60(8) [173.15]	170.05(8) [171.73]	173.0(1) [171.8]	172.99(9) [171.84]	172.9(1) [171.8]	172.14(6) [171.52]	

The initial entries in the table are the bond lengths obtained from x-ray structures with the estimated standard deviation presented in parenthesis. The values presented in square brackets are the bond lengths obtained from the DFT geometry optimized singlet ground state. The phenyl ring in the DFT geometry optimized singlet ground state of [PhSn(LBr)Cl₂] is 6.5 degrees from the Cl-Sn-Cl axis.

Table 2. Photophysical Data for all chromophores. All data was collected in acetonitrile.

Complex	[PhSn(Lnap) Cl ₂]	[PhSn(Lsal)C I ₂]	[PhSn(LBr)C I ₂]	[PhSn(Ldea)C I ₂]
Absorption λ_{\max} (nm)	452	424	434	462
Extinction Coefficient (M ⁻¹ cm ⁻¹)	20400	10800	11300	40700
Fluorescence λ_{\max} (nm)	524	532	541	602
Fluorescence λ_{\max} (cm ⁻¹)	19100	18800	18500	16600
Singlet Lifetime (ps), from TCSPC	1100 ± 100	660 ± 50	690 ± 40	----
^A Durbin-Watson Value (d)	2.47	2.41	2.11	----
^B Fluorescence Quantum Yield ± 10%	0.14	0.04	0.06	0.01
E ⁰ (+/0) (V)	1.25	1.34	1.38	0.83
E ⁰ (0/-) (V)	-1.37	-1.23	-1.27	-1.22
Triplet Lifetime in PMMA (ms)	0.98 ± 0.09	1.1 ± 0.3	0.57 ± 0.02	11.9 ± 1.3
Triplet energy, (cm ⁻¹) ± 300 cm ⁻¹	15,300	16,300	16,200	15,500
Intersystem Crossing Efficiency ± 10%	0.36	0.59	0.72	0.05
^C k _{isc} (s ⁻¹)	2.6 x 10 ⁸	7.4 x 10 ⁸	9.0 x 10 ⁸	3.1 x 10 ⁸
^C k _r (s ⁻¹)	7.5 x 10 ⁷	5.0 x 10 ⁷	7.5 x 10 ⁷	6.3 x 10 ⁷
^C k _{nr} (s ⁻¹)	3.6 x 10 ⁸	4.6 x 10 ⁸	2.8 x 10 ⁸	5.9 x 10 ⁹
Oxygen Quenching Rate Constant	2.1 x 10 ⁹	2.1 x 10 ⁹	2.2 x 10 ⁹	2.3 x 10 ⁹
^D Quantum Yield of ¹ O ₂ Generation ± 20%	0.43	0.52	0.66	----

(A) Durbin-Watson values were determined using the residual values obtained from a single exponential fit of deconvoluted luminescence intensity decays. Each decay was analyzed over 200 data points. (B) Fluorescence quantum yield values for [PhSn(Lsal)Cl₂], [PhSn(LBr)Cl₂], and [PhSn(Lnap)Cl₂] were determined with tetracene¹ as a reference and the value for

[PhSn(Ldea)Cl₂] was determined with [Ru(bpy)₃](PF₆)₂⁷⁵ as a reference. (C) Kinetic values determined using the long decay component obtained from the ultrafast transient absorption spectrum of each chromophore. (D) The quantum yield of ¹O₂ was determined with [Ru(bpy)₃](PF₆)₂⁵⁵ as a standard for all complexes.

Table 3. Kinetic Information Obtained from Femtosecond Transient Absorption Spectra

Complex	[PhSn(Lnap)Cl ₂]	[PhSn(Lsal)Cl ₂]	[PhSn(LBr)Cl ₂]	[PhSn(Ldea)Cl ₂]
τ ₁ (ps)	0.56 ± 0.05	0.75 ± 0.20	0.57 ± 0.12	0.13 ± 0.02
τ ₂ (ps)	70.0 ± 7.6	40.8 ± 8.5	40.4 ± 17	1.05 ± 0.20
τ ₃ (ps)	1390 ± 96	758 ± 66	767 ± 42	170 ± 17

References

- 1 S. L. Murov, I. Carmichael and G. L. Hug, *Handbook of Photochemistry*, New York (NY), 1993.
- 2 K. Oldenburg, A. Vogler and O. Horváth, *Inorg. Chim. Acta*, 1997, **257**, 149.
- 3 K. Oldenburg, A. Vogler, I. Miko and O. Horvath, *Inorg. Chim. Acta*, 1996, **248**, 107.
- 4 K. Oldenburg and A. Vogler, *Z. Naturforsch. , B: Chem. Sci.*, 1993, **48**, 1519.
- 5 H. Nikol, A. Becht and A. Vogler, *Inorg. Chem.*, 1992, **31**, 3277.
- 6 A. Volger and H. Nikol, *Pure Appl. Chem.*, 1992, **64**, 1311.
- 7 H. Kunkely and A. Vogler, *Chemical Physics Letters*, 1991, **187**, 609.
- 8 A. Vogler, A. Paukner and H. Kunkely, *Coord. Chem. Rev.*, 1990, **97**, 285.
- 9 H. Kim, W. Kim, Y. Mackeyev, G. Lee, H. Kim, T. Tachikawa, S. Hong, S. Lee, J. Kim, L. J. Wilson, T. Majima, P. J. J. Alvarez, W. Choi and J. Lee, *Environ. Sci. Technol.*, 2012, **46**, 9606.
- 10 W. Kim, T. Tachikawa, T. Majima, C. Li, H. Kim and W. Choi, *Energy Environ. Sci.*, 2010, **3**, 1789.
- 11 M. Martinez-Diaz, I. T. de and T. Torres, *Chem. Commun.*, 2010, **46**, 7090.
- 12 M. T. Indelli, C. Chiorboli, M. Ghirotti, M. Orlandi, F. Scandola, H. J. Kim and H. Kim, *J Phys Chem B*, 2010, **114**, 14273.
- 13 I. Seotsanyana-Mokhosi, T. Kresfelder, H. Abrahamse and T. Nyokong, *J. Photochem. Photobiol., B*, 2006, **83**, 55.
- 14 B. P. Rand, J. Xue, F. Yang and S. R. Forrest, *Appl. Phys. Lett.*, 2005, **87**, 233508.
- 15 S. Wang, I. Tabata, K. Hisada and T. Hori, *J. Porphyrins Phthalocyanines*, 2003, **7**, 199.
- 16 S. Wang, K. Enomoto, S. Tanizaki, I. Tabata, K. Hisada, T. Hori and S. Okubayashi, *Sen'i Gakkaishi*, 2003, **59**, 48.
- 17 S. Okubayashi, S. Ariga, H. Shosenji and T. Hori, *Sen'i Gakkaishi*, 1997, **53**, 431.
- 18 C. Grewer, G. Schermann, R. Schmidt, A. Voelcker, H. D. Brauer, A. Meier and F. P. Montforts, *J. Photochem. Photobiol., B*, 1991, **11**, 285.

- 19 A. R. Morgan, L. S. Cheng, D. Skalkos and G. M. Garbo, *Photochem. Photobiol.*, 1990, **52**, 987.
- 20 W. Szulbinski and J. W. Strojek, *Inorg. Chim. Acta*, 1986, **118**, 91.
- 21 J. Fuhrhop, W. Krüger and H. E. David, *Liebigs Ann. Chem.*, 1983, **1983**, 204.
- 22 P. Sayer, M. Gouterman and C. R. Connell, *Acc. Chem. Res.*, 1982, **15**, 73.
- 23 Y. Harel and J. Manassen, *J. Am. Chem. Soc.*, 1977, **99**, 5817.
- 24 M. Gouterman, F. P. Schwarz, P. D. Smith and D. Dolphin, *J. Chem. Phys.*, 1973, **59**, 676.
- 25 D. G. Whitten, J. C. N. Yau and F. A. Carroll, *J. Am. Chem. Soc.*, 1971, **93**, 2291.
- 26 R. S. Becker and J. B. Allison, *J. Phys. Chem.*, 1963, **67**, 2669.
- 27 M. Ohtani, P. V. Kamat and S. Fukuzumi, *J. Mater. Chem.*, 2010, **20**, 582.
- 28 J. Fortage, E. Goeransson, E. Blart, H. Becker, L. Hammarstroem and F. Odobel, *Chem. Commun.*, 2007, 4629.
- 29 C. Du, J. Yu, J. Huang and Y. Jiang, *Energy Procedia*, 2011, **12**, 519.
- 30 M. Idowu and T. Nyokong, *J. Photochem. Photobiol., A*, 2008, **199**, 282.
- 31 T. Nyokong, *J. Porphyrins Phthalocyanines*, 2008, **12**, 1005.
- 32 B. Agboola, K. I. Ozoemena and T. Nyokong, *J. Mol. Catal. A: Chem*, 2006, **248**, 84.
- 33 N. Nensala, A. Nzimande and T. Nyokong, *J. Photochem. Photobiol., A*, 1996, **98**, 129.
- 34 I. Aviv-Harel and Z. Gross, *Coord. Chem. Rev.*, 2011, **255**, 717.
- 35 I. Aviv and Z. Gross, *Chem. Commun.*, 2007, 1987.
- 36 D. Walker, S. Chappel, A. Mahammed, B. S. Brunshwig, J. R. Winkler, H. B. Gray, A. Zaban and Z. Gross, *J. Porphyrins Phthalocyanines*, 2006, **10**, 1259.
- 37 B. Ventura, A. D. Esposti, B. Koszarna, D. T. Gryko and L. Flamigni, *New J. Chem.*, 2005, **29**, 1559.
- 38 V. Pawlowski, H. Kunkely and A. Vogler, *Inorg. Chim. Acta*, 1995, **234**, 55.
- 39 V. Pawlowski, H. Kunkely and A. Vogler, *Coord. Chem. Rev.*, 1994, **132**, 23.

- 40 K. Makita, K. Nomura and Y. Saito, *J. Mol. Catal.*, 1994, **89**, 143.
- 41 T. Matsubara, Y. Saito, T. Yamakawa and S. Shinoda, *J. Mol. Catal.*, 1993, **79**, 29.
- 42 V. Pawlowski, H. Kunkely and A. Vogler, *J. Am. Chem. Soc.*, 1993, **115**, 7029.
- 43 T. Matsubara, Y. Saito, T. Yamakawa and S. Shinoda, *J. Mol. Catal.*, 1991, **67**, 175.
- 44 K. Nomura, Y. Saito and S. Shinda, *J. Mol. Catal.*, 1989, **50**, 303.
- 45 R. R. Andrea, L. De Wim G. J., D. J. Stufkens and A. Oskam, *Inorg. Chem.*, 1989, **28**, 318.
- 46 M. S. Holt, W. L. Wilson and J. H. Nelson, *Chem. Rev.*, 1989, **89**, 11.
- 47 J. D. Donaldson, *Prog. Inorg. Chem.*, 1968, **8**, 287.
- 48 K. Takano, M. Takahashi, T. Fukushima, M. Takezaki, T. Tominaga, H. Akashi, H. Takagi and T. Shibahara, *Bull. Chem. Soc. Jpn.*, 2012, **85**, 1210.
- 49 K. Takano and T. Shibahara, *Chem. Lett.*, 2008, **37**, 70.
- 50 C. Jiang, J. Wang and F. He, *Anal. Chim. Acta.*, 2001, **439**, 307.
- 51 A. Bondi, *J. Phys. Chem.*, 1964, **68**, 441.
- 52 V. Balzani, F. Bolletta and F. Scandola, *J. Am. Chem. Soc.*, 1980, **102**, 2152.
- 53 W. G. Herkstroeter and G. S. Hammond, *J. Am. Chem. Soc.*, 1966, **88**, 4769.
- 54 K. Sandros, *Acta Chem. Scand.*, 1964, **18**, 2355.
- 55 A. A. Abdel-Shafi, D. R. Worrall and A. Y. Ershov, *Dalton Trans.*, 2004, **2004**, 30.
- 56 S. R. Salman, S. K. Kanber and L. K. Arslian, *Spectrosc. Lett.*, 1990, **23**, 870.
- 57 K. A. Abbas, S. R. Salman, S. M. Kana'n and Z. A. Fataftah, *Can. J. Appl. Spectrosc.*, 1996, **41**, 119.
- 58 M. D. Cohen and G. M. J. Schmidt, *J. Phys. Chem.*, 1962, **66**, 2442.
- 59 M. D. Cohen, Y. Hirshberg and Schmidt G.M.J., *J. Chem. Soc.*, 1964, 2051.
- 60 M. Ottolenghi and D. S. McClure, *J. Chem. Phys.*, 1967, **46**, 4620.
- 61 R. Nakagaki, T. Kobayashi, J. Nakamura and S. Nagakura, *Bull. Chem. Soc. Jpn.*, 1977, **50**, 1909.

- 62 P. F. Barbara, P. M. Rentzepis and L. E. Brus, *J. Am. Chem. Soc.*, 1980, **102**, 2786.
- 63 R. S. Becker, C. Lenoble and A. Zein, *J. Phys. Chem.*, 1987, **91**, 3509.
- 64 W. Tuberville and P. K. Dutta, *J. Phys. Chem.*, 1990, **94**, 4060.
- 65 T. Yuzawa, H. Takahashi and H. Hamaguchi, *Chem. Phys. Lett.*, 1993, **202**, 221.
- 66 K. Kownacki, A. Mordzinski, R. Wilbrandt and A. Grabowska, *Chem. Phys. Lett.*, 1994, **227**, 270.
- 67 S. Mitra and N. Tamai, *Chem. Phys. Lett.*, 1998, **282**, 391.
- 68 P. Fita, E. Luzina, T. Dziembowska, D. Kopeć, P. Piątkowski, C. Radzewicz and A. Grabowska, *Chem. Phys. Lett.*, 2005, **416**, 305.
- 69 P. Fita, E. Luzina, T. Dziembowska, C. Radzewicz and A. Grabowska, *J. Chem. Phys.*, 2006, **125**, 184508.
- 70 U. Lachish, P. P. Infelta and M. Gratzel, *Chem. Phys. Lett.*, 1979, **62**, 317.
- 71 I. Carmichael and G. L. Hug, *J. Phys. Chem. Ref. Data*, 1986, **15**, 1.
- 72 Gaussian 09, Revision D.01, M. J. Frisch, G. W. Trucks, H. B. Schlegel, G. E. Scuseria, M. A. Robb, J. R. Cheeseman, G. Scalmani, V. Barone, B. Mennucci, G. A. Petersson, H. Nakatsuji, M. Caricato, X. Li, H. P. Hratchian, A. F. Izmaylov, J. Bloino, G. Zheng, J. L. Sonnenberg, M. Hada, M. Ehara, K. Toyota, R. Fukuda, J. Hasegawa, M. Ishida, T. Nakajima, Y. Honda, O. Kitao, H. Nakai, T. Vreven, J. A. Montgomery Jr., J. E. Peralta, F. Ogliaro, M. J. Bearpark, J. Heyd, E. N. Brothers, K. N. Kudin, V. N. Staroverov, R. Kobayashi, J. Normand, K. Raghavachari, A. P. Rendell, J. C. Burant, S. S. Iyengar, J. Tomasi, M. Cossi, N. Rega, N. J. Millam, M. Klene, J. E. Knox, J. B. Cross, V. Bakken, C. Adamo, J. Jaramillo, R. Gomperts, R. E. Stratmann, O. Yazyev, A. J. Austin, R. Cammi, C. Pomelli, J. W. Ochterski, R. L. Martin, K. Morokuma, V. G. Zakrzewski, G. A. Voth, P. Salvador, J. J. Dannenberg, S. Dapprich, A. D. Daniels, Ö. Farkas, J. B. Foresman, J. V. Ortiz, J. Cioslowski and D. J. Fox, Gaussian, Inc., Wallingford CT, 2009.
- 73 W. R. Wadt and P. J. Hay, *J. Chem. Phys.*, 1985, **82**, 284.
- 74 D. M. Collins, W. R. Scheidt and J. L. Hoard, *J. Am. Chem. Soc.*, 1972, **94**, 6689.
- 75 J. V. Caspar and T. J. Meyer, *J. Am. Chem. Soc.*, 1983, **105**, 5583.

